

Fusion mechanism in fullerene-fullerene collisions –The deciding role of giant oblate-prolate motion

J. Handt and R. Schmidt*

Institut für Theoretische Physik, Technische Universität Dresden, D-01062 Dresden, Germany

(Dated: June 17, 2021)

We provide answers to long-lasting questions in the puzzling behavior of fullerene-fullerene fusion: Why are the fusion barriers so exceptionally high and the fusion cross sections so extremely small? An *ab initio* nonadiabatic quantum molecular dynamics (NA-QMD) analysis of $C_{60}+C_{60}$ collisions reveals that the dominant excitation of an exceptionally “giant” oblate-prolate $H_g(1)$ mode plays the key role in answering both questions. From these *microscopic* calculations, a *macroscopic* collision model is derived, which reproduces the NA-QMD results. Moreover, it predicts *analytically* fusion barriers for different fullerene-fullerene combinations in excellent agreement with experiments.

PACS numbers: 36.40.-c

INTRODUCTION

After the pioneering $C_{60}+C_{60}$ collision experiment of E.E.B. Campbell et al. in 1993 [1], cluster-cluster collisions became a versatile new field of research (for reviews see [2–5]) with lasting interest [6–20]. In particular, fusion between fullerenes has been studied in great detail, both experimentally and theoretically [1, 21–37]. Fusion is a universal phenomenon in collisions between complex particles covering many orders in size and energy from heavy ion collisions in nuclear physics [38] to macroscopic liquid droplets [39, 40] or even colliding galaxies [41]. It is a great challenge of ongoing interest to reveal universal similarities and basic differences of these mechanisms.

Usually, the gross features of fusion can be understood with macroscopic arguments [10, 38, 40, 42] leading to the general expression for the fusion cross section σ as function of the center mass energy $E_{c.m.} \equiv E$ of

$$\sigma(E) = \pi R_{12}^2 \left(1 - \frac{V_B}{E}\right) \quad (1)$$

with $R_{12} = R_1 + R_2$ the sum of the radii of the colliding partners and V_B the fusion barrier (for a derivation see e.g. [3, 38, 43]). This formula (known as “critical distance model” in nuclear physics [38] or “absorbing sphere model” in chemistry [43]) describes *quantitatively* the experimental fusion cross section for atomic nuclei (with $V_B > 0$) and liquid droplets (with $V_B = 0$) [10, 39, 40] in the low energy range with $E \gtrsim V_B$ [44]. It is expected to hold also for collisions between metallic clusters [10] (even with $V_B < 0$); see last paper in the series [6–9]. The physics behind formula (1) is indeed simple: fusion takes place, if the colliding partners touch, owing to the larger binding energy of the fused compound [42]. For colliding fullerenes one naturally expects a fusion barrier V_B of at least the sp^2 bond breaking energy, or more pertinently the Stone-Wales transformation energy [33, 34] of a few eV [45] and, according to (1), a fusion cross section of the order of the geometrical one, $\pi R_{12}^2 \sim 150 \text{ \AA}^2$ [29]. Experimentally, however, the fusion barriers are about

one order of magnitude larger (around 80 eV) [29] and the cross sections are even two magnitudes smaller (a few Å^2) [31].

Up to now, there is no definite explanation for these findings, albeit some possible phenomenological reasons have been discussed [3–5, 31, 32]. In addition, previous (at that time still approximate) microscopic Quantum Molecular Dynamics (QMD) calculations predicted the large fusion barriers [28]. From these studies it is also well known that only very few mutual initial orientations of the colliding cages lead to fusion (without identifying them). Anyway, fullerenes typically do **not** fuse if they touch, even at high impact energies, and the question remains, why? In this work, we provide a clear answer to this longstanding question.

MICROSCOPIC RESULTS

Motivated by our recent findings of the dominating role of the $A_g(1)$ breathing mode in C_{60} -laser interaction [46, 47], we have reanalyzed fullerene-fullerene collisions with the help of the *ab initio* nonadiabatic quantum molecular (NA-QMD) method [48–51]. For systems as large as we are investigating here, NA-QMD is numerically more efficient than its *ab initio* QMD approximation [49–51]. In extension to previous studies [3, 27–29, 31] we include a normal mode analysis [52] of the vibrational kinetic energy. This method decomposes the total kinetic vibrational excitation energy E_{vib} into the individual contributions of all 174 eigenmodes of C_{60} as function of time t according to

$$E_{\text{vib}}(t) = \sum_{i=1}^{60} \frac{m_c}{2} \dot{\mathbf{r}}_i^2 = \sum_{\nu=1}^{174} \frac{m_c}{2} \left(\sum_{i=1}^{60} \dot{\mathbf{r}}_i \mathbf{b}_{i\nu} \right)^2$$

with the atomic carbon mass m_c , the atomic velocities $\dot{\mathbf{r}}_i$ (in the molecular center of mass system without rotational components) and the normal mode eigenvectors $\mathbf{b}_{i\nu}$.

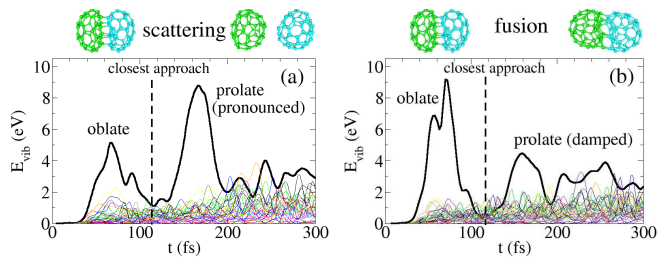


FIG. 1. (color online) Normal mode analysis of central $C_{60}+C_{60}$ collisions at an impact energy of $E_{c.m.} = 104$ eV. Shown are the vibrational kinetic energies E_{vib} of all 174 internal normal modes as function of time t for (a) typical scattering and (b) typical fusion events. Distances of closest approach R^{ret} are indicated by vertical, dashed lines. The dominating role of the $H_g(1)$ mode (black thick lines) is apparent.

In fig. 1, such an analysis, is shown for two central $C_{60}+C_{60}$ collisions with the same impact energy of $E_{c.m.} = 104$ eV but for different initial orientations of the clusters, leading in one case to scattering (fig. 1(a)) and, in the other, to fusion (fig. 1(b)). In both cases, the extraordinary dominance of the $H_g(1)$ mode is obvious.

During approach, this mode is very strongly excited to a much higher degree than any other vibrational mode. Its excitation energy of several eV is huge as compared to a single quantum of this mode of $\hbar\omega_{mode} \sim 34$ meV [53] and, thus, its amplitude is extremely large, as compared to a typical displacement of the elementary excitation (“giant” $H_g(1)$ mode). Consequently at the distance of closest approach R^{ret} , a highly deformed *oblate-oblate* configuration of the double cluster system is formed (see above illustrations in fig. 1). This clearly distinguishable state accommodates practically the whole impact energy into deformation (potential) energy, which is quantitatively shown in fig. 2(a), also for other impact energies. Up to this stage of the collision, there is no appreciable difference to the other collision systems (nuclei, droplets), where at this “critical distance” the system loses immediately its memory and the energy is dissipated into internal degrees of freedom (DOF) leading to a hot compound.

The fundamental difference to the other systems consists in the specific properties of the oblate-prolate mode in fullerenes and its special role in collisions. First of all, among all vibrational modes, the $H_g(1)$ mode in C_{60} has the largest oscillation period of $T = 122$ fs [53]. This is comparable with a typical collision time and therefore, once excited, this mode will *not* lose immediately its memory, as clearly seen in figs. 1(a) and 1(b). Second, the oblate-prolate mode is the only eigenmode which can couple directly to the relative motion via its elongated *prolate-prolate* configuration, provided it survives the dissipative coupling to all the other internal modes. This is exactly what happens in $C_{60}+C_{60}$ collisions and results in the majority of cases in scattering, like a *fis-*

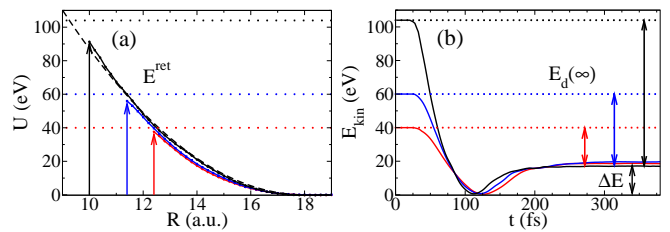


FIG. 2. (color online) Typical NA-QMD results for central $C_{60}+C_{60}$ collisions at impact energies of $E_{c.m.} = 40$ eV (red), 60 eV (blue), and 104 eV (black), indicated as dotted horizontal lines, and obtained by ensemble averaging over 20 different initial orientations. (a): The potential (deformation) energy of the relative motion $U(R)$ in the entrance channel as function of the distance R . The locations and lengths of the vertical arrows denote the distances of closest approach R^{ret} and the total deformation energy $E^{ret} \equiv U(R^{ret})$ stored at R^{ret} , respectively. The dashed line is the harmonic fit $U(R) = \frac{k}{2}(R - R^0)^2$ with $k = 0.12$ a.u. and $R^0 = 18.5$ a.u. (b): The kinetic energy of the relative motion E_{kin} as function of time t for scattering events. The mean values of the final kinetic energies $\Delta E \approx 17$ eV and of the corresponding energies dissipated into internal DOF $E_d(\infty) = E_{c.m.} - \Delta E$ are indicated by double arrows.

sion process with the *prolate-prolate* configuration at the scission point [42] (note the pronounced excitation of the mode in fig. 1(a) at $t \sim 165$ fs). Only strong coupling to the internal DOF can prevent this mechanism, allowing for fusion (note the strongly damped prolate oscillation of the mode in fig. 1(b) at $t \sim 165$ fs). Thus, the competitive coupling of the oblate-prolate mode to the relative motion and to all the other (bath-like) vibrational DOF determines the reaction channel !

The strength of the bath coupling is solely determined by the amount of energy stored in the mode at R^{ret} . This coupling dominates, if the energy exceeds a certain limit which generally can happen only at appropriate large impact energies. This explains (at least preliminarily and qualitatively) the high fusion barriers. At a fixed impact energy just above the barrier $E_{c.m.} \gtrsim V_B$ (as in fig. 1), only very rare and specific initial orientations of the clusters can lead to high $H_g(1)$ excitation energies, namely, those with the principal axes of the $H_g(1)$ mode aligned to the collision axis, ensuring maximal energy transfer, which is the case in the example shown in fig. 1(b) (note that E_{vib} of the mode during approach in the case of fusion (fig. 1(b)) is twice as large as compared to scattering (fig. 1(a))). This, finally, explains the low fusion cross sections and completes the present, new picture of the fusion mechanism.

It modifies also the hitherto existing interpretation of scattering, as a “bouncing off” mechanism [3, 4, 22, 28, 31], like in collisions between two soccer balls. Instead, “fission” via the prolate-prolate configuration strongly suggests, that the final kinetic energy of the fragments is largely independent on impact energy. This is nicely

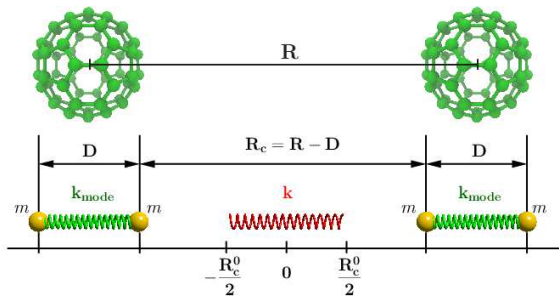


FIG. 3. (color online) Phenomenological collision model with two DOF, the distance between the centers $R(t)$ and the diameter $D(t)$ of the fullerenes: Two collinear colliding springs (with spring constants k_{mode} and masses m) interact during approach via a third, massless spring (spring constant k and initial length R_c^0) located at the collision center.

confirmed in the calculations and shown in fig. 2(b).

The collision scenario presented in figs. 1 and 2 is characteristic for fullerene-fullerene reactions and qualitatively observed in our NA-QMD calculations also for the other combinations and finite, small impact parameters. Despite its microscopic complexity, the mechanism is nevertheless simple and can be understood and described by ordinary *macroscopic* concepts, as will be shown in the following.

COLLISION MODEL

The basic idea is to reduce drastically the 360-dimensional scattering problem to a one-dimensional one with only two, but relevant collective DOF, treated explicitly in a time-dependent fashion: the distance between the centers $R(t)$ (relative motion) and the diameters of the fullerenes $D(t)$ (aligned along their principal axes of the oblate-prolate mode). Both are coupled via the contact distance $R_c = R - D$ (see fig. 3). The coupling to the other internal DOF will be treated implicitly in the exit channel only. The macroscopic model is designed as follows:

(i) In the entrance channel, the system consists of two collinear colliding springs with initial lengths $D(t=0) = D^0$, spring constants k_{mode} and masses $m = \frac{M}{2}$ at the ends (describing the fullerenes with mass M and their $H_g(1)$ modes). Tightly located in between there is a third, massless spring with initial length R_c^0 and constant k , describing the repulsive potential U during approach (remember fig. 2(a) and see fig. 3 and fig. 4(a)).

(ii) In the exit channel, the massless repulsive spring is replaced by a “dissipative” potential U_d , which describes the coupling to all other internal vibrational DOF, and hence, controls the reaction channel (see fig. 4(b)).

The coupled Newton equations in the entrance channel

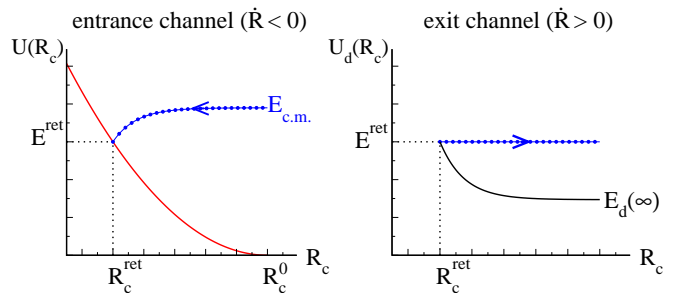


FIG. 4. (color online) Schematic plot of the potential energy in the entrance channel $U(R_c)$ (left) and, for the case of scattering, in the exit channel $U_d(R_c)$ (right) as function of the contact distance R_c . Dotted blue lines with directional arrows indicate a typical trajectory (idealized as a straight line in the exit channel) with impact energy $E_{c.m.}$ at the initial distance R_c^0 and potential energy E^{ret} at the distance of closest approach R_c^{ret} . The asymptotic value of the potential energy in the exit channel $U_d(R_c \rightarrow \infty) \equiv E_d(\infty)$ is also indicated.

read

$$\begin{aligned} \mu \ddot{R} &= - \left. \frac{dU}{dR_c} \right|_{R_c=R-D} \\ \mu_{\text{mode}} \ddot{D} &= - \frac{dV_{\text{mode}}}{dD} + \frac{1}{2} \left. \frac{dU}{dR_c} \right|_{R_c=R-D} \end{aligned} \quad (2)$$

with the reduced masses $\mu = \frac{M}{2}$ and the mass constant $\mu_{\text{mode}} = \frac{M}{4}$. The harmonic potentials are given by $U(R_c) = \frac{k}{2}(R_c - R_c^0)^2$ with $k = 0.12$ a.u. (see fig. 2(a)) and $V_{\text{mode}}(D) = \frac{k_{\text{mode}}}{2}(D - D^0)^2$ with the spring constant $k_{\text{mode}} = \mu_{\text{mode}} \omega_{\text{mode}}^2 = 0.51$ a.u., obtained from the experimental frequency of the $H_g(1)$ mode in C_{60} ($\omega_{\text{mode}} = 273 \text{ cm}^{-1}$ [53]). The equations of motion (EOM) (2) can be solved analytically (see appendix). They describe the collision up to the distance of closest approach, i.e., the classical returning point R_c^{ret} . At this point the potential $U(R_c)$ for $R_c > R_c^{\text{ret}}$ is replaced by the “dissipative” one $U_d(R_c)$ which, in dependence on $E_{c.m.}$, controls the outcome. It is therefore repulsive (leading in any case to scattering) or attractive (leading usually to fusion, but not necessarily always). Thus, it has the general form

$$U_d(R_c) = (E^{\text{ret}} - E_d(\infty)) f(R_c - R_c^{\text{ret}}) + E_d(\infty) \quad (3)$$

where the form factor f must fulfill the conditions, $f(0) = 1$ (ensuring the continuity of the potential at R_c^{ret}) and $f(\infty) = 0$ (making sure that the maximal amount of dissipated energy cannot exceed $E_d(\infty)$, in the case of scattering). In fact, the concrete radial dependence of the potential (3) is not relevant, and thus, we choose a simple exponential form of $f(x) = \exp(-\frac{x}{\Delta})$ with $\Delta = \left| \frac{R_c^{\text{ret}} - R_c^0}{2} \left(1 - \frac{E_d(\infty)}{E^{\text{ret}}} \right) \right|$, which guarantees also continuity of the force at R_c^{ret} in the case of scattering.

With this, all model parameters (k , k_{mode} , ΔE) are fixed and the EOM (2) can be easily solved numerically.

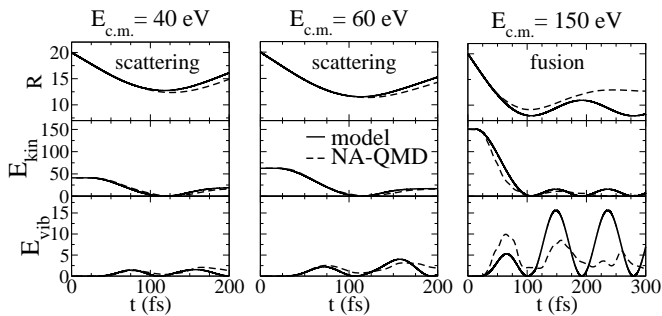


FIG. 5. Comparison between NA-QMD (dashed lines) and model calculations (solid lines) for central $C_{60}+C_{60}$ collisions at three impact energies $E_{c.m.}$: distance between the centers R in a.u. (top), kinetic energy of the relative motion E_{kin} (middle), and vibrational kinetic energy of the $H_g(1)$ mode E_{vib} (bottom) in eV as function of time t .

The results are shown in fig. 5 and compared with NA-QMD calculations (for movies see www.dymol.org).

The model reproduces nearly precisely the microscopic calculations for both scattering ($E_{c.m.} = 40, 60$ eV) and fusion ($E_{c.m.} = 150$ eV). The ongoing oscillations of some quantities in the exit channel are the natural consequence of the absence of a damping mechanism for the $H_g(1)$ mode in the spring model. The most impressive result, however, concerns the fusion barrier predicted by the model of $V_B = 85$ eV, which is in excellent agreement with former (extremely expensive) QMD calculations [28] of $V_B = 80$ eV.

ANALYTICAL SOLUTION FOR THE FUSION BARRIER

The simplicity of the EOM (2) and the transparency of the ansatz (3) encouraged us to further elaborate the model and to demonstrate its predictive power. As mentioned already, the EOM (2) can be solved analytically, and, from this solution one can derive an approximate expression for the energy stored during approach E^{ret} (see Fig 4(a)), resulting in a linear dependence on the impact energy of $E^{ret} = \alpha(\kappa) E_{c.m.}$ with κ the ratio of the spring constants

$$\kappa = \frac{k_{mode}}{k} = \frac{M\omega_{mode}^2}{4k} \quad (4)$$

and the universal function $\alpha(\kappa)$ of

$$\alpha(\kappa) = \frac{1}{4(\kappa^2 + 1)} \left[\frac{\kappa - 1 - \sqrt{\kappa^2 + 1}}{\sqrt{\kappa + 1} + \sqrt{\kappa^2 + 1}} \right. \\ \left. \times \sin\left(\frac{\pi}{2} \frac{\kappa + 1 + \sqrt{\kappa^2 + 1}}{\sqrt{2\kappa}}\right) - \frac{\kappa - 1 + \sqrt{\kappa^2 + 1}}{\sqrt{\kappa + 1} - \sqrt{\kappa^2 + 1}} \right]^2 \quad (5)$$

(see appendix). The difference $(E^{ret} - E_d(\infty))$ determines the (positive or negative) slope of the potential U_d (3) at the returning point R_c^{ret} . Taking an idealized trajectory as shown in fig. 4 (i.e., neglecting the acceleration of the mode near the barrier), the fusion condition simply reads $E^{ret} \stackrel{!}{=} E_d(\infty)$ at $E_{c.m.} = V_B$. With $E_d(\infty) = E_{c.m.} - \Delta E$ (see fig. 2(b)), the fusion barrier becomes

$$V_B = \frac{\Delta E}{1 - \alpha(\kappa)}. \quad (6)$$

For $C_{60}+C_{60}$ collisions, this approximate expression gives $V_B = 82$ eV, which is very close to the exact model value ($V_B = 85$ eV) obtained in the upper dynamical calculations. To obtain a first insight about the qualitative trends for the other combinations ($C_{60}+C_{70}$, $C_{70}+C_{70}$), we ignore subtleties and use the same k and ΔE values as obtained already for $C_{60}+C_{60}$ by NA-QMD fine tuning. The internal spring constant for C_{70} , however, is carefully chosen and fixed again by experiment. From the (partly) non-degenerate five $H_g(1)$ modes in C_{70} (E'_2, E''_1, A'_1) an experimental mean value of $\omega_{mode}(C_{70}) = 261 \text{ cm}^{-1}$ has been reported [54] giving the spring constant $k_{mode}(C_{70}) = 0.55$ a.u. For the (slightly) asymmetric $C_{60}+C_{70}$ collision a reasonable mean value of $k_{mode}(C_{60})$ and $k_{mode}(C_{70})$ of $k_{mode}(C_{60}/C_{70}) = 0.53$ a.u. is used.

With these parameters, the predicted fusion barriers from (6) are compared with high precision QMD values [28], in table I (first two rows). The analytical model reproduces the right trend and delivers absolute values within 10% accuracy. Obviously, the $H_g(1)$ frequencies ω_{mode} and fullerene masses M , eq. (4) determine the fusion barriers in fullerene-fullerene collisions.

This is strongly supported by comparing the predictions with experimental data. In this case, the finite temperature ($T \approx 2000$ K) of the colliding fullerenes has to be taken into account [29]. This has been done in the former QMD calculations [28] and led to the (well known) perfect agreement with the experimental data (cf. third and fifth rows in table I). In the present model, a finite temperature can be naturally taken into account by reducing the mode frequencies ω_{mode} . Using an arbitrary common scaling factor for k_{mode} of 0.85, the predicted fusion barriers by eq. (6) are in beautiful agreement with the experiment (fourth and fifth row in table I).

CONCLUSION

To summarize, *ab initio* NA-QMD studies have finally cleared up the fusion mechanism in fullerene-fullerene collisions. The excitation of a “giant” $H_g(1)$ mode explains both large fusion barriers and small fusion cross sections. This *microscopic* picture is non-ambiguously confirmed by a *macroscopic* spring model which depicts

TABLE I. Fusion barriers V_B in eV for various fullerene-fullerene combinations as predicted by our former QMD calculations [28] (first and third rows) and the present analytical model (second and fourth rows). The experimental values [29] are presented in the last row.

	$T = 0$ K		$T = 2000$ K		exp.
	QMD model	QMD model	QMD model	QMD model	
C ₆₀ +C ₆₀	80	82	60	65	60±1
C ₆₀ +C ₇₀	94	87	70	69	70±6.5
C ₇₀ +C ₇₀	104	93	75	73	76±4

clearly the physics, reproduces the NA-QMD results and the experimental fusion barriers *quantitatively*.

We note finally, that a “giant” vibrational excitation of the $A_g(1)$ breathing mode in C₆₀ has been found recently in a time-resolved laser experiment [46]. The general investigation of large amplitude motion in fullerenes, including laser-induced *fission* [47], could become an interesting new field of research.

APPENDIX: ANALYTICAL SOLUTION IN THE ENTRANCE CHANNEL

Inserting the harmonic potentials $U(R_c)$ and $V(D)$, the EOM (2) can be written as

$$\begin{aligned} \mu \ddot{R} &= -k (R_c - R_c^0) \Big|_{R_c=R-D} \\ \mu_{\text{mode}} \ddot{D} &= -k_{\text{mode}} (D - D^0) + \frac{k}{2} (R_c - R_c^0) \Big|_{R_c=R-D} \end{aligned} \quad (\text{A.1})$$

which can be solved by making an exponential ansatz $e^{i\Omega t}$. Doing so, the fundamental eigenfrequencies $\Omega_{1/2}$ of the system read

$$\Omega_{1/2} = \omega \underbrace{\sqrt{\kappa + 1 \pm \sqrt{\kappa^2 + 1}}}_{f_{1/2}(\kappa)} \quad (\text{A.2})$$

with the frequency $\omega = \sqrt{\frac{k}{\mu}}$ and the force constant ratio κ as defined in eq. (4).

With the initial conditions

$$\begin{aligned} R(0) &\equiv R^0 = D^0 + R_c^0, & \dot{R}(0) &= v_{\text{c.m.}}, \\ D(0) &= D^0, & \dot{D}(0) &= 0 \end{aligned}$$

the solution of (A.1) is given by

$$R(t) = \frac{v_{\text{c.m.}}}{\omega} \sum_{i=1,2} a_i \sin(\Omega_i t) + R^0, \quad (\text{A.3})$$

$$D(t) = \frac{v_{\text{c.m.}}}{\omega} \sum_{i=1,2} b_i \sin(\Omega_i t) + D^0 \quad (\text{A.4})$$

with the amplitudes $a_{1/2} = \frac{1}{2 f_{1/2}(\kappa)} (1 \mp \frac{\kappa}{\sqrt{\kappa^2+1}})$ and $b_{1/2} = \mp \frac{1}{2 f_{1/2}(\kappa)} \frac{1}{\sqrt{\kappa^2+1}}$.

With the analytical solution (A.3), (A.4) the potential energy at the returning point E^{ret} can be calculated. E^{ret} is given by

$$E^{\text{ret}} \equiv U(R_c^{\text{ret}}) = \frac{k}{2} (R_c^{\text{ret}} - R_c^0)^2 \quad (\text{A.5})$$

with $R_c^{\text{ret}} \equiv R_c(t^{\text{ret}}) = R(t^{\text{ret}}) - D(t^{\text{ret}})$.

The returning time t^{ret} defined by $\dot{R}(t^{\text{ret}}) = 0$ is approximated by $t^{\text{ret}} \approx \frac{\pi}{2\Omega_2}$. The approximation is justified since the second term of the sum in eq. (A.3) dominates for the parameter range of κ used here ($\frac{a_1}{a_2} \ll 1$).

Inserting the analytical solution (A.3), (A.4) in the definition (A.5) and using the relation (A.2) we find

$$E^{\text{ret}} = \alpha(\kappa) E_{\text{c.m.}}$$

with the impact energy $E_{\text{c.m.}} = \frac{\mu}{2} v_{\text{c.m.}}^2$ and the coefficient $\alpha(\kappa)$ as defined before in eq. (5).

We thank Sebastian Schmidt (ETH Zurich) for many useful comments and critical reading of the manuscript. We gratefully acknowledge the allocation of computer resources from ZIH and MPI-PKS, Dresden and appreciate the support of the DFG through Einzelverfahren.

* Corresponding author; Ruediger.Schmidt@tu-dresden.de

- [1] E. E. B. Campbell, V. Schyja, R. Ehlich, and I. V. Hertel, *Phys. Rev. Lett.*, **70**, 263 (1993).
- [2] R. Schmidt and H. Lutz, *Comments At. Mol. Phys.*, **31**, 461 (1995).
- [3] O. Knospe and R. Schmidt, in *Theory of Atomic and Molecular Clusters*, edited by J. Jellinek (Springer, 1999) p. 111.
- [4] E. E. B. Campbell and F. Rohmund, *Rep. Prog. Phys.*, **63**, 1061 (2000).
- [5] E. E. B. Campbell, *Fullerene Collision Reactions* (Kluwer Academic Publishers, Dordrecht, 2003).
- [6] R. Schmidt, G. Seifert, and H. O. Lutz, *Physics Letters A*, **158**, 231 (1991).
- [7] G. Seifert, R. Schmidt, and H. O. Lutz, *Physics Letters A*, **158**, 237 (1991).
- [8] O. Knospe, R. Schmidt, E. Engel, U. Schmitt, R. Dreizler, and H. Lutz, *Physics Letters A*, **183**, 332 (1993).
- [9] R. Schmidt and H. Lutz, *Physics Letters A*, **183**, 338 (1993).
- [10] R. Schmidt and H. O. Lutz, *Phys. Rev. A*, **45**, 7981 (1992).
- [11] R. Schmidt, J. Schulte, O. Knospe, and G. Seifert, *Phys. Lett. A*, **194**, 101 (1994).
- [12] J. Schulte, O. Knospe, G. Seifert, and R. Schmidt, *Phys. Lett. A*, **198**, 51 (1995).
- [13] F. Zhang, F. Spiegelmann, E. Suraud, V. Frayssé, R. Poteau, R. Glowinski, and F. Chatelin, *Physics Letters A*, **193**, 75 (1994).
- [14] H. Shen, P. Hvelplund, D. Mathur, A. Bárány, H. Cedergquist, N. Selberg, and D. C. Lorents, *Phys. Rev. A*, **52**, 3847 (1995).
- [15] B. Farizon, M. Farizon, and M. J. Gaillard, *Int. J. Mass Spectrom.*, **192**, 259 (1999).

- [16] H. Bräuning, R. Trassl, A. Diehl, A. Theiß, E. Salzborn, A. A. Narits, and L. P. Presnyakov, *Phys. Rev. Lett.*, **91**, 168301 (2003).
- [17] J. Rogan, R. Ramírez, A. H. Romero, and M. Kiwi, *Eur. Phys. J. D*, **28**, 219 (2004).
- [18] O. Kamalou, B. Manil, H. Lebius, J. Rangama, B. Huber, P. Hvelplund, S. Tomita, J. Jensen, H. Schmidt, H. Zettergren, and H. Cederquist, *Int. J. Mass Spectrom.*, **252**, 117 (2006).
- [19] D. Alamanova, V. G. Grigoryan, and M. Springborg, *J. Phys.: Condensed Matter*, **19**, 346204 (2007).
- [20] J. Jakowski, S. Irle, B. G. Sumpter, and K. Morokuma, *J. Phys. Chem. Letters*, **3**, 1536 (2012).
- [21] C. Yeretzian, K. Hansen, F. Diederich, and R. L. Whetten, *Nature*, **359**, 44 (1992).
- [22] D. L. Strout, R. L. Murry, C. Xu, W. C. Eckhoff, G. K. Odum, and G. E. Scuseria, *Chem. Phys. Lett.*, **576**, 214 (1993).
- [23] B. L. Zhang, C. T. Wang, C. Chan, and K. M. Ho, *J. Phys. Chem.*, **97**, 3134 (1993).
- [24] S. G. Kim and D. Tománek, *Phys. Rev. Lett.*, **72**, 2418 (1994).
- [25] D. H. Robertson, D. W. Brenner, and C. T. White, *J. Phys. Chem.*, **99**, 15721 (1995).
- [26] Y. Xia, Y. Xing, C. Tan, and L. Mei, *Phys. Rev. B*, **53**, 13871 (1996).
- [27] F. Rohmund, E. E. B. Campbell, O. Knospe, G. Seifert, and R. Schmidt, *Phys. Rev. Lett.*, **76**, 3289 (1996).
- [28] O. Knospe, A. V. Glotov, G. Seifert, and R. Schmidt, *J. Phys. B*, **29**, 5163 (1996).
- [29] F. Rohmund, A. V. Glotov, K. Hansen, and E. E. B. Campbell, *J. Phys. B*, **29**, 5143 (1996).
- [30] Y. Xia, Y. Mu, C. Tan, Y. Xing, and H. Yang, *Nucl. Instr. and Meth. in Phys. Res. Sec. B*, **129**, 356 (1997).
- [31] A. Glotov, O. Knospe, R. Schmidt, and E. E. B. Campbell, *Eur. Phys. J. D*, **16**, 333 (2001).
- [32] E. E. B. Campbell, A. V. Glotov, A. Lassesson, and R. D. Levine, *C. R. Physique*, **3**, 341 (2002).
- [33] Y. Zhao, R. E. Smalley, and B. I. Yakobson, *Phys. Rev. B*, **66**, 195409 (2002).
- [34] S. Han, M. Yoon, S. Berber, N. Park, E. Osawa, J. Ihm, and D. Tománek, *Phys. Rev. B*, **70**, 113402 (2004).
- [35] N. Kaur, K. Dharamvir, and V. Jindal, *Chem. Phys.*, **344**, 176 (2008).
- [36] J. Jakowski, S. Irle, and K. Morokuma, *Phys. Rev. B*, **82**, 125443 (2010).
- [37] Y. Wang, H. Zettergren, P. Rousseau, T. Chen, M. Gatchell, M. H. Stockett, A. Domaracka, L. Adoui, B. A. Huber, H. Cederquist, M. Alcamí, and F. Martín, *Phys. Rev. A*, **89**, 062708 (2014).
- [38] R. Bock, *Heavy Ion Collisions*, Vol. 1-3 (North-Holland, Amsterdam, 1980).
- [39] G. Brenn and A. Frohn, *Exp. Fluids*, **7**, 441 (1989).
- [40] A. Menchaca-Rocha, F. Huidobro, A. Martinez-Davalos, K. Michaelian, A. Perez, V. Rodriguez, and N. Cárjan, *J. Fluid Mech.*, **346**, 291 (1997).
- [41] C. Struck, *Physics Reports*, **321**, 1 (1999).
- [42] R. W. Hasse and W. D. Myers, *Geometrical Relationships of Macroscopic Nuclear Physics* (Springer-Verlag Berlin, 1988).
- [43] R. D. Levine and R. B. Bernstein, *Molecular Reaction Dynamics and Chemical Reactivity* (Oxford University Press, New York, 1987).
- [44] We do not consider here the high energy range, where the cross sections generally decreases with $E_{c.m.}$, see [10].
- [45] M. S. Dresselhaus, G. Dresselhaus, and P. C. Eklund, *Science of Fullerenes and Carbon Nanotubes* (Academic Press, San Diego, 1996).
- [46] T. Laarmann, I. Shchatsinin, A. Stalmashonak, M. Boyle, N. Zhavoronkov, J. Handt, R. Schmidt, C. P. Schulz, and I. V. Hertel, *Phys. Rev. Lett.*, **98**, 058302 (2007).
- [47] M. Fischer, J. Handt, G. Seifert, and R. Schmidt, *Phys. Rev. A*, **88**, 061403(R) (2013).
- [48] T. Kunert and R. Schmidt, *Eur. Phys. J. D*, **25**, 15 (2003).
- [49] M. Fischer, J. Handt, and R. Schmidt, *Phys. Rev. A*, **90**, 012525 (2014).
- [50] M. Fischer, J. Handt, and R. Schmidt, *Phys. Rev. A*, **90**, 012526 (2014).
- [51] M. Fischer, J. Handt, and R. Schmidt, *Phys. Rev. A*, **90**, 012527 (2014).
- [52] G. P. Zhang and T. F. George, *Phys. Rev. Lett.*, **93**, 147401 (2004).
- [53] Z.-H. Dong, P. Zhou, J. M. Holden, P. C. Eklund, M. S. Dresselhaus, and G. Dresselhaus, *Phys. Rev. B*, **48**, 2862 (1993).
- [54] X. Q. Wang, C. Z. Wang, and K. M. Ho, *Phys. Rev. B*, **51**, 8656 (1995).